Co-published by
Institute of Fluid-Flow Machinery
Polish Academy of Sciences
Committee on Thermodynamics and Combustion
Polish Academy of Sciences

Copyright©2026 by the Authors under licence CC BY-NC-ND 4.0

http://www.imp.gda.pl/archives-of-thermodynamics/

Impact of activation energy and Deborah number on heat and mass transfer of three dimensional rotating magnetic nanofluid over a stretching surface

P. Sudarsana Reddy*, P. Sreedevi

Department of Mathematics, Rajeev Gandhi Memorial College of Engineering & Technology, Nandyal-518501, A.P, India
*Corresponding author email: suda1983@gmail.com

Received: 26.07.2025; revised: 27.04.2026; accepted: 10.08.2026

Abstract

The influence of activation energy and thermal Biot number on MHD (magnetohydrodynamic) mass and heat transport analysis of rotating Maxwell nanoliquid flow over an elongating surface with radiation is examined in the present study by considering both suction and non-suction cases. Momentum equations in both directions of x and y, energy and species equations are transformed into the a of ODEs (ordinary differential equations) by utilising similarity conversions. These transformed equations supplemented with boundary conditions are solved numerically with the use of the finite element method. Velocities in both x and y directions, concentration and temperature sketches are plotted for various values of Deborah parameter, activation energy, Biot number, magnetic parameter, thermophoresis, Brownian motion, radiation and rotation parameters. The rates of mass transport, heat transport and dimensionless gradient of velocity are also calculated. Key findings reveal that an increase in activation energy significantly enhances the concentration of the nanoliquid in both suction and non-suction cases. Furthermore, it was observed that the magnetic parameter induces a Lorentz force that retards fluid motion while simultaneously elevating the liquid's temperature. Results also demonstrate that the rotation parameter has a more pronounced effect on temperature degradation in the presence of suction.

Keywords: Rotating fluid; Maxwell nanofluid; MHD; Convective boundary condition; Finite element method; Radiation

Vol. 47(2026), No. 3, 241–252; doi: 10.24425/ather.2026.7524

Cite this manuscript as: Sudarsana Reddy, P., & Sreedevi, P. (2026). Impact of activation energy and Deborah number on heat and mass transfer of three dimensional rotating magnetic nanofluid over a stretching surface. *Archives of Thermodynamics*, 47(3), 241–252.

1. Introduction

Cancer therapy, energy production, cooling of nuclear reactors, power generation, thermal insulation, food processing, storage of foodstuffs, increasing the efficiency of engines, etc., are a few industrial and environmental applications of nanoliquids. Limited thermal conductivity is the major drawback of common liquids like engine oil, kerosene, water and ethylene glycol. Their thermal conductivities may amplify by adding a kind of metal particles known as “nanoparticles”. The thermal conductivity of such nanoliquids is enhanced compared to normal liquids. Recently, many authors worked on and calculated the heat transport performance of dissimilar kinds of nanoliquids and observed considerable augmentation of heat transfer in nanofluids [1–10].

Mass and heat transport features of Maxwell nanoliquid have also received highest priority by the research community, as it has good applications in electronic devices. Recent advancements in renewable energy systems have highlighted the critical role of nanofluids in enhancing the efficiency of photovoltaic-

Nomenclature

B_0 – magnetic field strength, T
B1 – Biot number
C_f – skin-friction coefficient
Cr – chemical reaction parameter
D_B – Brownian diffusion coefficient, m^2/s
D_T – thermophoretic diffusion coefficient, m^2/s
$E1$ – activation energy parameter
$f(\eta)$– dimensionless stream function
g – gravitational acceleration, m/s^2
k_{nf} – thermal conductivity of nanofluid, W/(m·K)
k_o^2 – chemical reaction rate
k_s – thermal conductivity, W/(m·K)
K – porous parameter
K^* – mean absorption coefficient
Le – Lewis number
M – magnetic parameter
Nb – Brownian motion parameter
Nt – thermophoresis parameter
Nu_x– Nusselt number
Pr – Prandtl number
q_r – radiative heat flux, W/m^2
q_w – wall heat flux, W/m^2
R – radiation parameter
T – fluid temperature, K
T_w – surface temperature, K
T_∞ – ambient temperature, K
u, v– velocity components in x- and y-axis, m/s
$V0$ – suction parameter
x, y – Cartesian coordinates, m

Greek symbols

α – thermal diffusivity of base fluid, m^2/s
β – thermal expansion coefficient, 1/K
ε – pressure parameter
η – similarity variable
θ_η – dimensionless temperature
λ – Maxwell parameter
μ – fluid viscosity, Pa·s
μ_{nf} – kinematic viscosity of the nanofluid, Pa·s
ν_f – kinematic viscosity of the base fluid, m^2/s
ρ_f – density of the base fluid, kg/m^3
ρ_{nf} – density of the nanofluid, kg/m^3
ρ_p – nanoparticle mass density, kg/m^3
σ – electrical conductivity, S/m
σ^* – Stephan-Boltzmann constant, $W/(m^2 \cdot K^4)$
τ_w – shear stress, Pa
φ – volume fraction of nanoparticles
ϕ_η – dimensionless concentration
ψ – stream function
Ω – rotation parameter

Subscripts and Superscripts

f – base fluid
nf – nanofluid
w – at the cone surface
∞ – far away from the cone surface

Abbreviations and Acronyms

FEM – finite element method
MHD– magnetohydrodynamics
ODE – ordinary differential equation

thermal (PVT) systems. Advanced configurations, such as the use of nanofluid spectral splitters to improve concentrated solar PV thermal efficiency and the integration of thermoelectric generators supported by nanofluid filters, have shown great promise for sustainable energy production. Furthermore, the inclusion of vortex generators in the presence of heat sinks has been shown to significantly influence the performance of concentrated solar modules. Ahmed et al. [11] investigated heat transport and flow features of a Buongiorno modelled Maxwell nanoliquid over a shrinking/stretching radially rotating disk by taking variable thermal conductivity into account and observed that the thermophoresis parameter deteriorates heat transport in the nanoliquid. Ijaz et al. [12] investigated the authority of double stratification and activation energy on species and energy transport topographies of Maxwell nanoliquid over an inclined non-linear stretching cylinder and professed that the velocity profiles of the Maxwell nanoliquid decrease with the increasing values of the Deborah parameter. Ahmed et al. [13] presented Buongiorno typed nanoliquid concentration and temperature features over a revolving disk with uniform injection/suction and observed that the rate of mass transport magnifies with magnifying values of the thermophoresis number. Ahmed et al. [14,15] deliberated the Buongiorno modelled Maxwell nanoliquid flow behaviour over a disk/cylinder in which the resulting non-linear fluid flow equations are numerically examined by utilising MATLAB built in function bvp4c. Sharma et al. [16] discussed the sway of viscous dissipation and Joule heating on flow analysis of graphene Maxwell nanoliquid over a non-linearly extending sheet and observed that the rate of heat transport augments as the values of thermal slip number amplify. Khan et al. [17] professed non-Newtonian Maxwell nanoliquid flow over an exponential widening surface and observed that the rate of heat transport values decreases with the increasing values of time relaxation number. Abro et al. [18] analysed SWCNTs (single-walled carbon nanotubes) and MWCNTs (multi-walled carbon nanotubes), ethylene glycol type Maxwell nanoliquid heat transport features and observed magnification in the rates of energy transport of Maxwell nanoliquid with amplifying nanoparticle volume fraction values. Ali et al. [19] deliberated copper/alumina typed Maxwell hybrid nanoliquid flow features through a vertical channel and intuited that amplification in the values of volume fraction of both considered nanoparticles elevates the temperature scatterings of the nanofluid. Jamshed et al. [20] investigated the sway of MHD and entropy generation on energy and flow features of Maxwell nanoliquid, prepared with copper–H_2O/titanium oxide–H_2O, over a horizontal infinite plate and detected a noticeable increase in the thermal conductivity of the nanofluid compared with the base liquid. Gowda et al. [21] deliberated Maxwell-Casson modelled nanoliquid heat transport and flow analysis between double elongated disks. Zhou et al. [22] analysed fluid flow topographies of Maxwell thermally radiative nanoliquid over a rotating stretchable porous disk.

Mustafa et al. [23] pondered the influence of Christov-Cattaneo energy flux on heat transport and flow examination over a stretching surface and observed that as the values of thermal relaxation number increase, the temperature of the liquid decreases. Ahuja et al. [24] analysed the influence of magnetic field and rotation parameter on fluid flow of rotating Maxwell nanofluid. Hayat et al. [25] implemented the optimal homotopy analysis method to investigate mass and energy transport in rotating Maxwell nanoliquid over a spreading exponential surface, and observed that the nanoliquid temperature magnifies with the increasing values of Deborah number. Rashid et al. [26] investigated the power of chemical reaction and Arrhenius energy on three-dimensional rotating Maxwell nanofluid heat transport performance over an exponentially widening porous surface and observed amplification in the sketches of temperature with magnifying values of heat sink/source number. Ali et al. [27] investigated mass and heat transport of three-dimensional rotating Maxwell nanoliquid flow over a stretchable surface with activation energy and Christov-Cattaneo double diffusion and observed that the temperature scattering of the nanoliquid magnifies with amplifying values of the Deborah parameter. Ahmed et al. [28] perceived the sway of Christov-Cattaneo double diffusion on solutal and thermal energy transport of rotating Maxwell nanoliquid flow over a revolving disk. Khalid et al. [29] pondered the impact of thermophoresis and Brownian motion on Rayleigh-Benard convective rotating Maxwell nanoliquid flow saturated with permeable media. Ramaiah et al. [30] examined the transport of mass and flow of revolving Maxwell nanoliquid over a stretchable sheet with activation energy and Christov-Cattaneo heat flux, and observed denigration in the scatterings of temperature as the Deborah number values amplify. Khan et al. [31], in their work on flow analysis of revolving Maxwell nanoliquid over an exponential/linear stretched sheet, scrutinised that as the values of rotation parameter magnifies, the heat flux of the nanoliquid is increased. Ali et al. [32] investigated solutal and heat energy transport features of bio-convective Maxwell revolving nanoliquid over a Riga plate with Christov-Cattaneo heat flux and observed magnification in the temperature of the liquid with the growing value of rotation parameter. Chu et al. [33] professed the sway of Newtonian heating and gyrotactic microorganisms on heat transport and flow investigation of revolving Maxwell nanoliquid over an elongated surface. Alzahrani et al. [34] pondered radiative Maxwell nanoliquid flow behaviour over a revolving frame by captivating microorganisms and activation energy into consideration and observed a magnification in the liquid temperature with the enhanced rotation parameter values. Very recently, Cao et al. [35], Wei et al. [36] and Ali et al. [37] studied the thermophysical properties of rotating Maxwell nanoliquid flow over various configurations and observed that the effect of Deborah number is considerably high on the velocity and rates of heat transport in the liquid. Very recently, several authors [38–41] studied heat and mass transport of tri-nanoliquids over different geometries and noticed considerable augmentation in the rates of heat transfer after adding nanoparticles to the base fluid.

Careful examination of the aforementioned literature [11–37] reveals that while several researchers have explored rotating Maxwell nanoliquid flows, a comprehensive analysis of mass and energy transport in a three-dimensional rotating Maxwell radiative nanoliquid over an exponentially stretching sheet, specifically incorporating the combined effects of activation energy and the thermal Biot number, is currently missing. This study aims to fill this significant gap by investigating these coupled phenomena. The governing non-linear equations are conversed using similarity transformations and solved numerically using the finite element method (FEM). The novelty of this work lies in providing a detailed understanding of how activation energy and convective boundary conditions influence the performance of rotating non-Newtonian systems, with results presented for both suction and non-suction cases.

2. Mathematical modelling of the problem

Consider the steady, three-dimensional, rotating, viscous, incompressible, laminar, MHD boundary layer Maxwell nanofluid flow past an exponentially stretching surface. The coordinate system is chosen such that *u*, *v* and *w* are the velocity components along the *x*-, *y*- and *z*- directions, respectively, as shown in Fig. 1. We also consider a constant magnetic field of strength in the *z*-direction. The flow is caused by the stretching of the sheet, which moves in its own plane with the surface velocity. The stretching surface is maintained at a uniform temperature and concentration, and these values are assumed to be greater than the ambient temperature and concentration, respectively. Under the above assumptions and with reference to the work of Hayat et al. [25], the governing equations describing the momentum, energy and concentration in the presence of thermal radiation, activation energy and chemical reaction take the following form:

$$\frac{\partial u}{\partial x}+\frac{\partial v}{\partial y}+\frac{\partial w}{\partial z}=0, \tag{1}$$

$$u\frac{\partial u}{\partial x}+v\frac{\partial u}{\partial y}+w\frac{\partial u}{\partial z}-2\Omega v=\frac{\mu}{\rho}\frac{\partial^2 u}{\partial z^2}-\lambda_1\left(u^2\frac{\partial^2 u}{\partial x^2}+v^2\frac{\partial^2 u}{\partial y^2}+w^2\frac{\partial^2 u}{\partial z^2}+2uv\frac{\partial^2 u}{\partial x\,\partial y}+2vw\frac{\partial^2 u}{\partial y\,\partial z}+\right.$$
$$\left.+2uw\frac{\partial^2 u}{\partial x\,\partial z}-2\Omega\left(u\frac{\partial v}{\partial x}+v\frac{\partial v}{\partial y}+w\frac{\partial v}{\partial z}\right)+2\Omega\left(v\frac{\partial u}{\partial x}-u\frac{\partial u}{\partial y}\right)\right)-\frac{\sigma}{\rho}{B_0}^2u, \tag{2}$$

$$u\frac{\partial v}{\partial x}+v\frac{\partial v}{\partial y}+w\frac{\partial v}{\partial z}+2\Omega u=\frac{\mu}{\rho}\frac{\partial^2 v}{\partial z^2}-\lambda_1\left(u^2\frac{\partial^2 v}{\partial x^2}+v^2\frac{\partial^2 v}{\partial y^2}+w^2\frac{\partial^2 v}{\partial z^2}+2uv\frac{\partial^2 v}{\partial x\,\partial y}+2vw\frac{\partial^2 v}{\partial y\,\partial z}+\right.$$
$$\left.+2uw\frac{\partial^2 v}{\partial x\,\partial z}+2\Omega\left(u\frac{\partial u}{\partial x}+v\frac{\partial u}{\partial y}+w\frac{\partial u}{\partial z}\right)+2\Omega\left(v\frac{\partial v}{\partial x}-u\frac{\partial u}{\partial y}\right)\right)-\frac{\sigma}{\rho}{B_0}^2v, \tag{3}$$

$$u\frac{\partial T}{\partial x}+v\frac{\partial T}{\partial y}+w\frac{\partial T}{\partial z}=\alpha\frac{\partial^2 T}{\partial z^2}+\tau\left[D_B\frac{\partial C}{\partial z}\frac{\partial T}{\partial z}+\left(\frac{D_T}{T_\infty}\right)\left(\frac{\partial T}{\partial z}\right)^2\right]-\frac{1}{\rho c_p}\frac{\partial q_r}{\partial z}, \quad (4)$$

$$u\frac{\partial C}{\partial x}+v\frac{\partial C}{\partial y}+w\frac{\partial C}{\partial z}=D_B\frac{\partial^2 C}{\partial z^2}-k_o^2\left(\frac{T}{T_0}\right)^n(C-C_\infty)e^{\frac{-E1}{\kappa T}}. \quad (5)$$

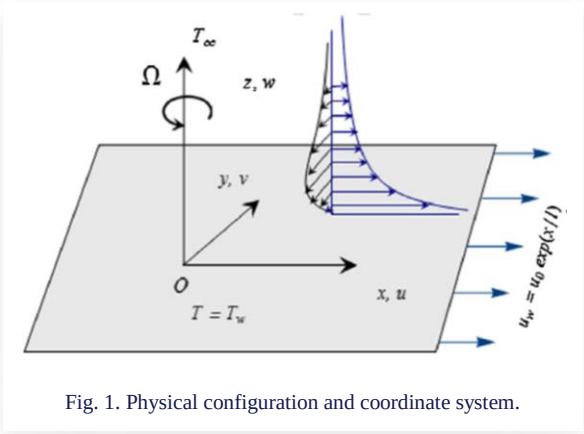


Fig. 1. Physical configuration and coordinate system.

The associated boundary conditions are:

$$C=C_w,\ -k\frac{\partial T}{\partial y}=h_f\left(T_f-T\right),\ u=u_w(x)=U_0e^{(x/L)},$$

$$v=0,\ w=-U_0 \text{ at } z=0;$$

$$C\to C_\infty,\ v\to 0,\ T\to T_\infty,\ u\to 0 \text{ at } z\to\infty. \quad (6)$$

By utilising the Rosseland diffusion approximation, the radiative heat flux is defined as:

$$q_r=-\frac{4\sigma^*}{3K^*}\frac{\partial T^4}{\partial y}. \quad (7)$$

We assume that the temperature variations within the fluid region are sufficiently small so that T^4 can be approximated as a linear function of T; therefore, this term can be expanded in a Taylor series. After neglecting higher-order terms in the expansion of the Taylor series of T^4 about T_∞, we obtain:

$$T^4\cong 4T_\infty{}^3T-3T_\infty^4. \quad (8)$$

After replacing Eq. (8) in Eq. (7), we obtain:

$$q_r=-\frac{16T_\infty{}^3\sigma^*}{3K^*}\frac{\partial T}{\partial z}. \quad (9)$$

The subsequent similarity transformations are considered to convert the above non-linear PDEs (partial differential equations) into ODEs.

$$v=U_0e^{\left(\frac{x}{L}\right)}\omega(\eta),\ u=U_0e^{\left(\frac{x}{L}\right)}f'(\eta),$$

$$w=-\left(\frac{U_0\nu}{2L}\right)^{\frac{1}{2}}e^{\left(\frac{x}{2L}\right)}\left(f(\eta)+\omega(\eta)\right),$$

$$\phi(\eta)=\frac{C-C_\infty}{C_w-C_\infty},\ \theta(\eta)=\frac{T-T_\infty}{T_w-T_\infty},\ \eta=\left(\frac{U_0}{2\nu L}\right)^{\frac{1}{2}}e^{\left(\frac{x}{2L}\right)}z. \quad (10)$$

Substituting Eqs. (9) and (10) into Eqs. (1)–(5), we get the subsequent non-linear ODEs:

$$f'''+ff''-2f'^2-\frac{\beta}{2}(f^2f'''-6ff'f''-\eta f'^2f''+4f'^3)-Mf'+\lambda(4\omega-2\beta(f\omega'+\eta f''\omega)=0, \quad (11)$$

$$\omega''+f\omega'-2f'\omega-\frac{\beta}{2}\left(f^2\omega''-6ff'^{\omega'}-\eta f'^2\omega'+4f'^2\omega\right)-Mf'+4\lambda\left(-f'+\beta\left(-f'^2-\omega^2-\frac{\eta}{2}\omega\omega'+\frac{1}{2ff''}\right)\right)=0, \quad (12)$$

$$(1+R)\theta''+\mathrm{Pr}f\theta'-\mathrm{Pr}Af'\theta+Nb\theta'\phi'+Nt(\theta')^2=0, \quad (13)$$

$$\phi''+\mathrm{Le}f\phi'-\mathrm{Le}Bf'\phi-Cr(1+\delta\theta)^ne^{\left(\frac{-E1}{(1+\delta\theta)}\right)}\phi+\frac{Nt}{Nb}\theta''=0. \quad (14)$$

The transformed boundary conditions are:

$$\eta=0,\ f=V0,\ \omega=0,\ f'=1,\ \theta'=-\mathrm{B1}(1-\theta),\ \phi=1;$$

$$\eta\longrightarrow\infty,\ \theta=0,\ f'=0,\ \omega=0,\ \phi=0, \quad (15)$$

where

$$\beta=\frac{\lambda_1U_w}{L},\ Nt=\frac{\tau D_T(T_w-T_\infty)}{\alpha T_\infty},\ Nb=\frac{\tau D_B(C_w-C_\infty)}{\alpha},\ \lambda=\frac{\Omega L}{U_w},$$

$$\delta=\frac{T_w-T_\infty}{T_\infty},\ V0=\frac{-V_wx}{\alpha(U_0/2\nu L)^{0.5}},\ \mathrm{Le}=\frac{\gamma}{D_B},\ Cr=\frac{k^2{}_o}{\alpha},\ \mathrm{Pr}=\frac{\gamma}{\alpha},$$

$$R=\frac{16T_\infty{}^3\sigma^*}{3K^*k_f},\ M=\frac{\sigma\beta_0^2}{\rho\,\alpha},\ \mathrm{B1}=\frac{h_f}{k(U_0/2\nu L)^{0.5}}. \quad (16)$$

Quantities of practical interest in this problem are the skin-friction coefficient (C_f), local Nusselt number (Nu_x), and the local Sherwood number (Sh_x), which are defined as:

$$\mathrm{C_f}=\frac{2\tau_w}{\rho},\ \mathrm{Nu_x}=\frac{xq_w}{k(T_w-T_\infty)},\ \mathrm{Sh_x}=\frac{xJ_w}{D_B(c_w-c_\infty)}. \quad (17)$$

3. Method of solution

The set of non-linear ODEs Eqs. (11)–(14) together with boundary conditions Eq. (15) are solved using the finite element method [42–46], which is highly efficient for boundary layer problems. The procedure involves the following steps:

Discretization: The entire domain [0, $\eta_{\max}$] is divided into a finite number of linear or quadratic sub-elements. We selected $\eta_{\max}$ = 4 as the infinity boundary, ensuring that all profiles asymptotically reach their required values.

Weighted residuals: The Galerkin method is applied to the governing equations to derive the weak form.

Shape functions: Linear interpolation functions are used to approximate the primary variables (velocity, temperature, concentration).

Assembly and iterations: The element stiffness matrices are assembled into a global matrix. Since the system is non-linear, an iterative approach is used with convergence criterion of 10^{-6} for all variables.

The 0.01 size taken refers to the dimensionless element length ($\Delta\eta$). Within the domain $\eta = [0,4]$, this results in 500 equal elements, providing high resolution for the boundary layer.

4. Results and discussion

This section presents the comparison of concentration, temperature and velocity scatterings for dissimilar values of pertinent parameters with ($V0 \neq 0$) or without ($V0 = 0$) suction. The values of the species concentration gradient, gradient of temperature and velocity are also investigated and presented in the form of Tables. The current calculations were validated by comparing the present results with the existing results, as shown in Table 1. To verify the convergence of the numerical solution, the grid independence test is performed and demonstrated in Table 2.

Table 1. Comparison of Nusselt number and Sherwood number values with existing results.

Parameter		Hayat et al. [25]		Present results	
β	λ	$-\theta'(0)$	$-\phi'(0)$	$-\theta'(0)$	$-\phi'(0)$
0.0	**0.1**	0.5323	0.5040	0.5328	0.5043
0.1	**0.1**	0.5239	0.4943	0.5232	0.4946
0.2	**0.1**	0.5172	0.4858	0.5174	0.4854
0.1	**0.0**	0.5358	0.5107	0.5355	0.5102
0.1	**0.1**	0.5239	0.4943	0.5231	0.4945
0.1	**0.2**	0.4988	0.4609	0.4986	0.4607

Table 2. Grid independence analysis of the problem.

Number of elements	Step size ($\Delta\eta$)	$f''(0)$	$-\theta'(0)$	$-\phi'(0)$
100	0.05	1.23456	0.45678	0.78901
250	0.02	1.23561	0.45712	0.78955
500	0.01	1.23565	0.45715	0.78958
1000	0.005	1.23565	0.45715	0.78958

The impact of magnetic number (M) on the sketches of velocity in x-direction (f'), velocity in y-direction (ω), temperature (θ) and concentration (ϕ) with suction ($V0 \neq 0$) and without ($V0 = 0$) is exposed in Figs. 2–5. The velocity profiles in the x- and y-directions both decrease with the increasing values of M, and this diminishing nature is more pronounced in the case of $V0 = 0$ than in the case of $V0 \neq 0$, as shown in Figs. 2 and 3. Both temperature and concentration sketches magnify with intensifying values of M and this magnification is considerably higher in the case of $V0 \neq 0$ than in the case of $V0 = 0$, as depicted in Figs. 4 and 5. This occurs because the application of a magnetic field to the fluid flow generates a Lorentz force. This force opposes the fluid motion, thereby reducing the velocity of the liquid. To dominate this force, fluid has to perform additional work, which causes an increase in temperature of the liquid.

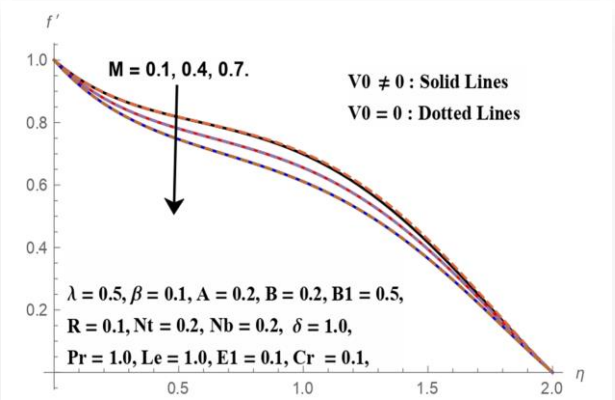


Fig. 2. Effect of M on f'.

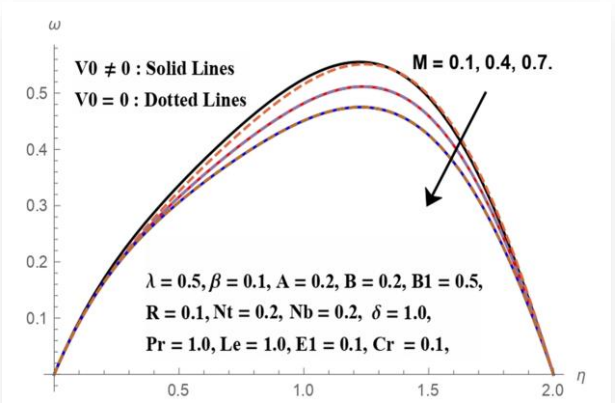


Fig. 3. Effect of M on ω.

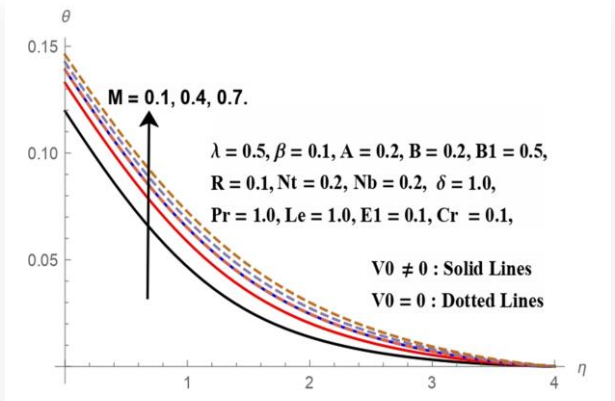


Fig. 4. Effect of M on θ.

Temperature and concentration profiles, in both cases $V0 \neq 0$ and $V0 = 0$, for dissimilar values of rotation number (λ) are illustrated in Figs. 6 and 7. The sketches of temperature of rotating nanoliquid decrease with the amplifying values of λ, and this decreasing trend is more pronounced in the case of $V0 \neq 0$ than in the case of $V0 = 0$. Furthermore, the concentration profiles of the nanoliquid also decrease as λ increases, and this decrease is more pronounced for $V0 \neq 0$ than for $V0 = 0$.

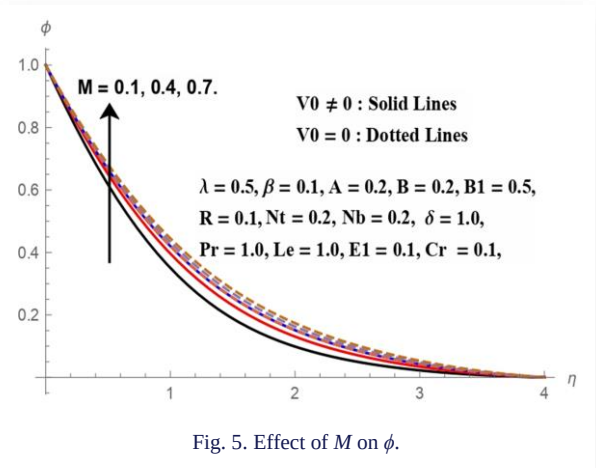


Fig. 5. Effect of M on ϕ.

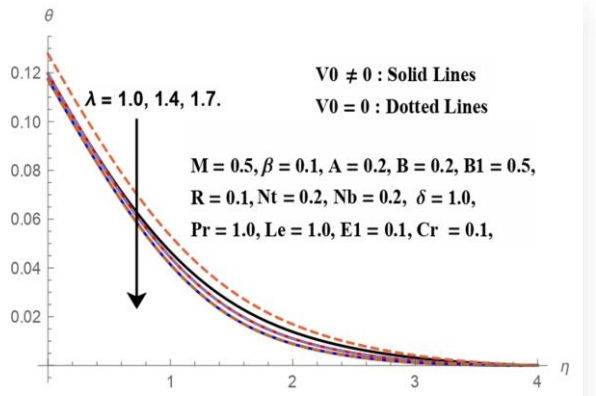


Fig. 6. Effect of λ on θ.

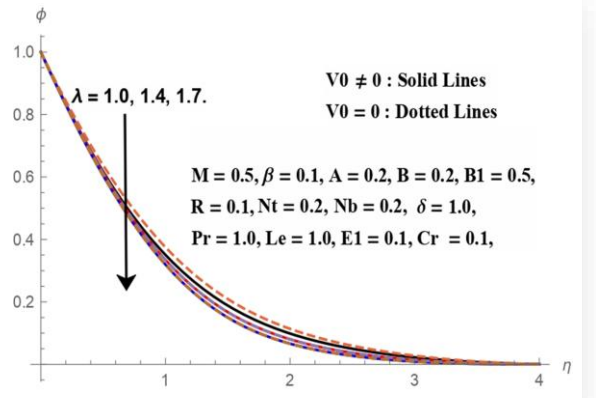


Fig. 7. Effect of λ on ϕ.

The Deborah parameter (β) influence on the distributions of velocity (f') in x-direction, velocity (ω) in y-direction, temperature (θ) and concentration (ϕ) with suction ($V0 \neq 0$) and without suction ($V0 = 0$) is disclosed in Figs. 8–11. Both components of velocity distributions of rotating nanoliquid diminish with the magnifying values of β in both cases of $V0 \neq 0$ and $V0 = 0$. This is true, generally because the Deborah number (β) is contingent on the relaxation time, and values of the Maxwell nanofluid relaxation time upsurge with the rising Deborah number values; therefore, the velocity of the rotating nanoliquid declines in the liquid area. However, the temperature and concentration of the rotating nanoliquid both magnify with the increasing values of β as revealed in Figs. 10 and 11.

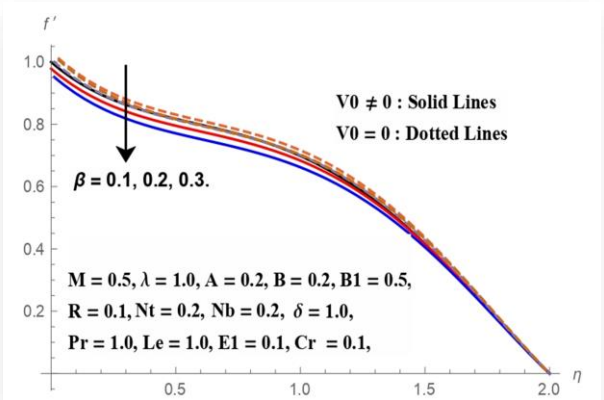


Fig. 8. Effect of β on f'.

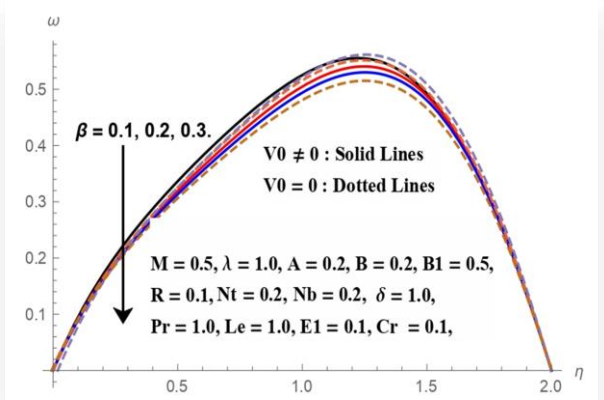


Fig. 9. Effect of β on ω.

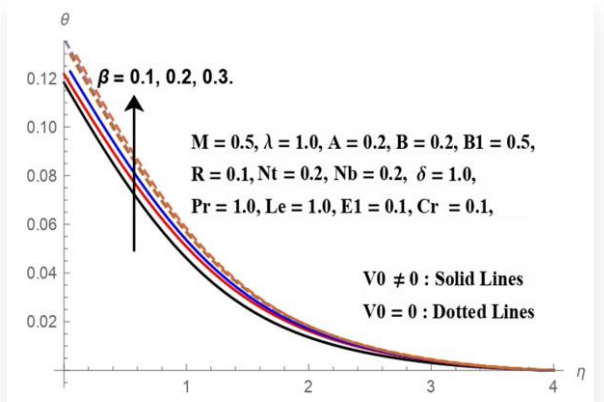


Fig. 10. Effect of β on θ.

The thermal radiation number (R) increases the temperature of the rotating Maxwell nanofluid in both cases of $V0 \neq 0$ and $V0 = 0$, as illustrated in Fig. 12. Generally, the inclusion of thermal radiation increases the fluid temperature. This increase in temperature profiles is slightly greater for the case of $V0 = 0$ than in the case of $V0 \neq 0$. Furthermore, the distributions of concent-

ration also increase with the rising R values in both cases of suction and without suction (Fig. 13).

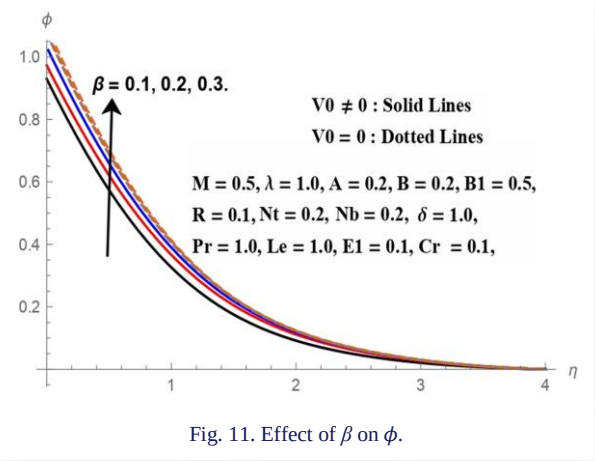


Fig. 11. Effect of β on ϕ.

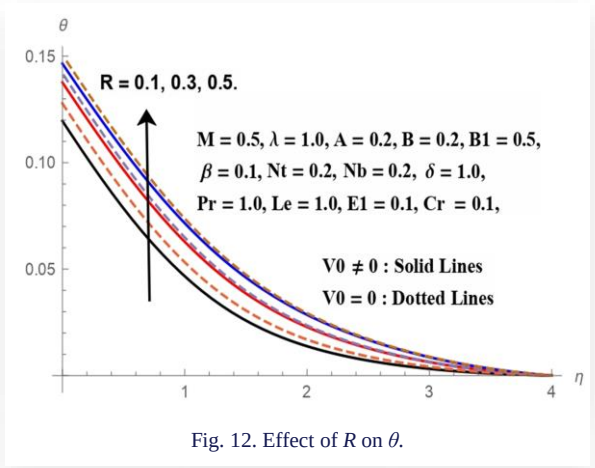


Fig. 12. Effect of R on θ.

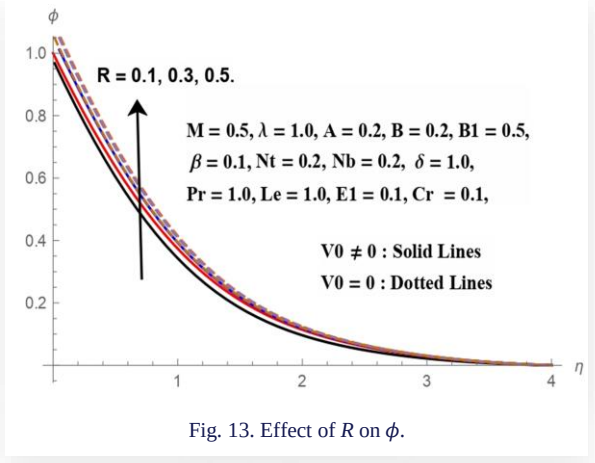


Fig. 13. Effect of R on ϕ.

The temperature and concentration fields of the rotating Maxwell nanoliquid for different values of the Brownian motion parameter Nb are shown in Figs. 14–15 for both $V0 \neq 0$ and $V0 = 0$. The temperature profiles increase with the increasing Nb, and this increase is slightly greater for $V0 = 0$ than for $V0 \neq 0$. In contrast, the concentration profiles decrease as Nb increases. Generally, nanoparticles undergo random motion in the fluid region (Brownian motion), which increases the fluid temperature and is also associated with nanoparticle agglomeration and size.

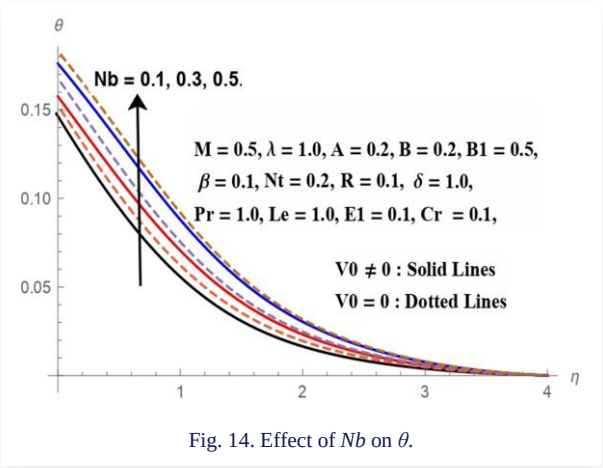


Fig. 14. Effect of Nb on θ.

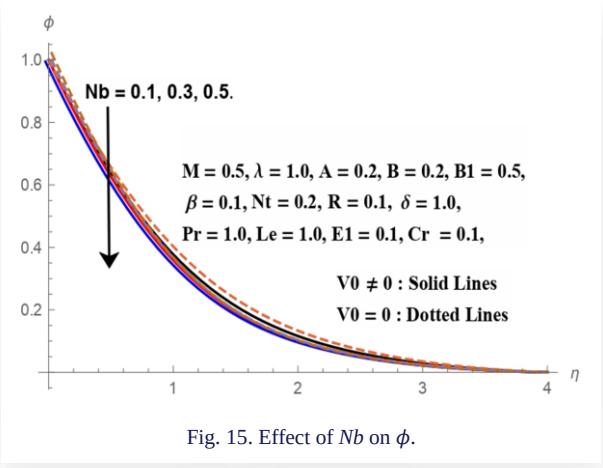


Fig. 15. Effect of Nb on ϕ.

Figs. 16–17 illustrate that both temperature and concentration profiles of rotating Maxwell nanoliquid increase with the rising thermophoretic parameter (Nt) values in both cases with and without suction. This is because the thermophoretic forces influentially thrust the particles present at the hot surface towards the cold surface; as a consequence, both the temperature and concentration of the rotating Maxwell nanoliquid magnify.

The chemical reaction parameter (Cr) impact on species outlines of rotating Maxwell nanofluid is depicted in Fig.18 in both cases with and without suction. The concentration profiles of the rotating Maxwell nanoliquid decrease with the increasing Cr, and this decrease is slightly greater for $V0 \neq 0$ than for $V0 = 0$. The effect of the Lewis number Le on the concentration profiles is illustrated in Fig. 19. The concentration distributions decrease in both cases with the increasing values of Le.

The concentration profiles of the rotating Maxwell nanofluid increase with the increasing values of the activation energy parameter ($E1$), as shown in Fig. 20, for both $V0 \neq 0$ and $V0 = 0$. Figure 21 shows that the concentration profiles of the rotating Maxwell nanoliquid increase as the temperature ratio parameter (δ) increases in both the suction and non-suction cases.

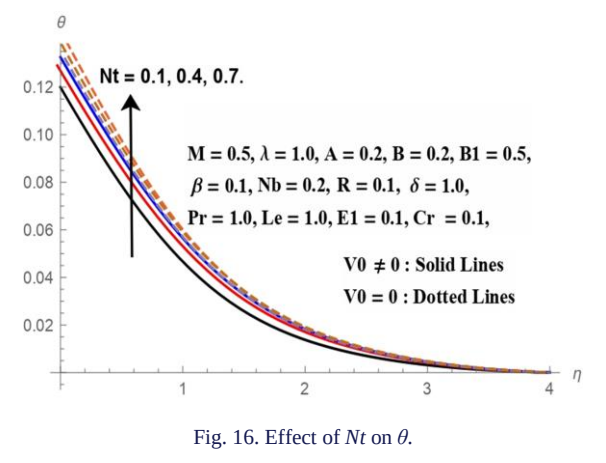


Fig. 16. Effect of *Nt* on θ.

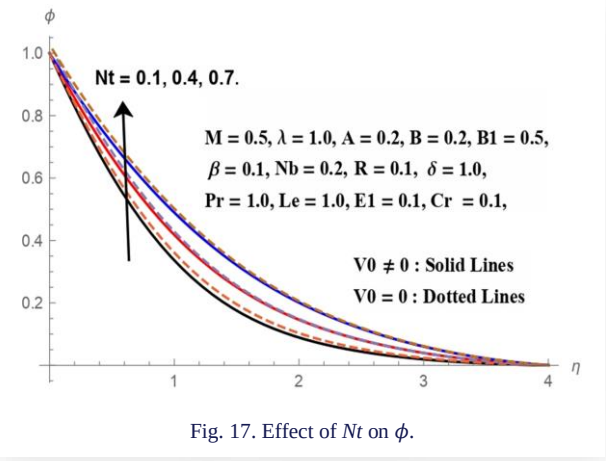


Fig. 17. Effect of *Nt* on ϕ.

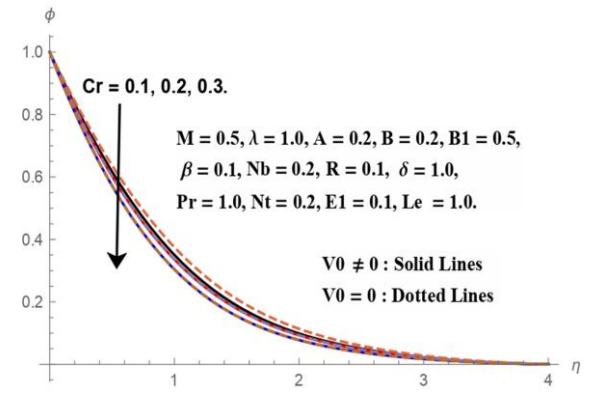


Fig. 18. Effect of *Cr* on ϕ.

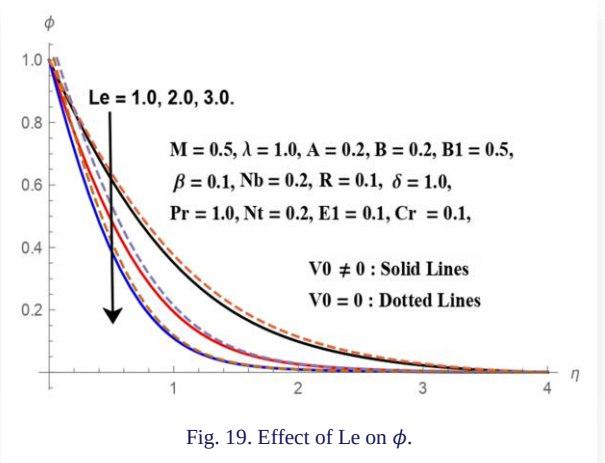


Fig. 19. Effect of Le on ϕ.

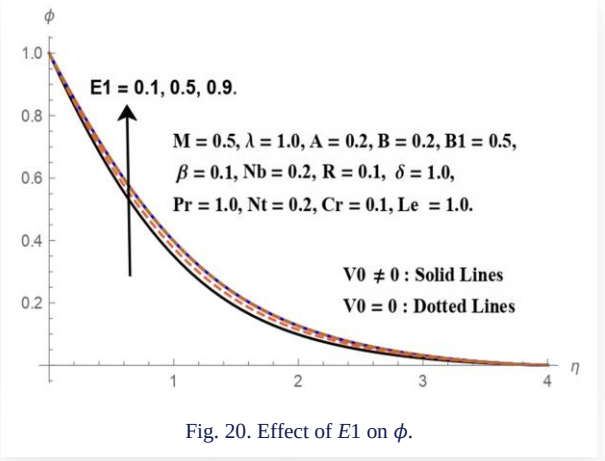


Fig. 20. Effect of *E*1 on ϕ.

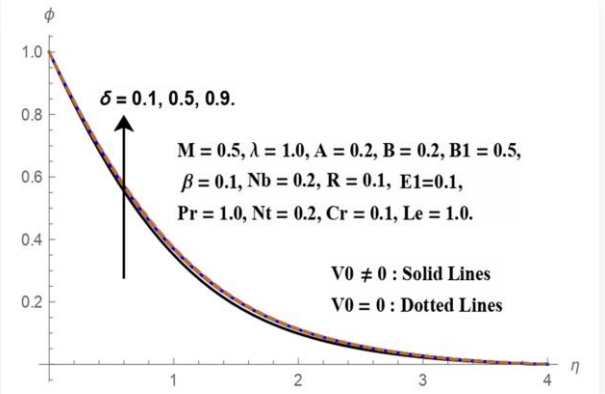


Fig. 21. Effect of δ on ϕ.

As the temperature exponent parameter (*A*) increases, the temperature profiles of the rotating Maxwell nanoliquid decrease, and this decrease is more pronounced for $V0 \neq 0$ than for $V0 = 0$, as illustrated in Fig. 22. Figure 23 shows that the concentration profiles of the rotating Maxwell nanoliquid decrease as the concentration exponent parameter (*B*) increases, with a slightly greater decrease for $V0 \neq 0$ than for $V0 = 0$.

The effect of the thermal Biot number B1 on the temperature and concentration profiles of the rotating Maxwell nanoliquid is illustrated in Figs. 24–25 for both $V0 \neq 0$ and $V0 = 0$. The temperature profiles increase with the increasing B1, and this increase is more pronounced for $V0 = 0$ than for $V0 \neq 0$. Furthermore, the concentration distributions increase with the increasing B1 in both cases.

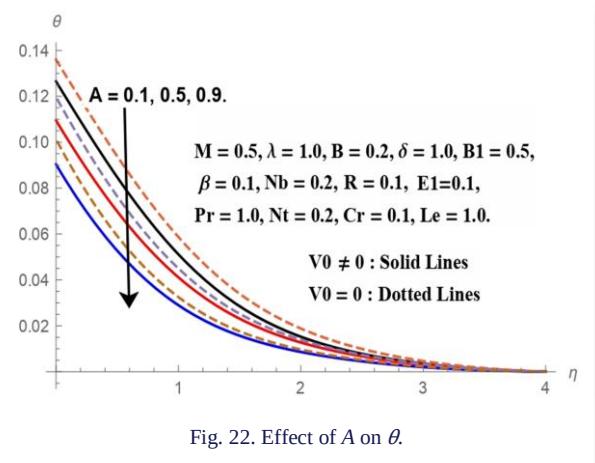


Fig. 22. Effect of A on θ.

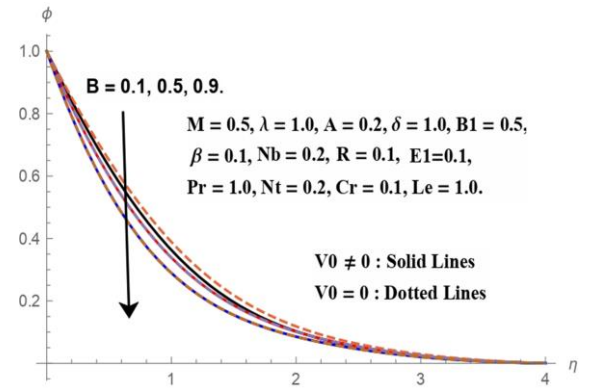


Fig. 23. Effect of B on ϕ.

The effects of various pertinent parameters on the velocity gradient, Sherwood number, and heat transfer under both suction and non-suction conditions are presented in Tables 3 and 4. It is observed that the dimensionless rates of mass, heat, and momentum transfer of the rotating Maxwell nanoliquid decrease with the increasing values of M in both the suction and non-suction cases. Furthermore, the concentration gradient and velocity gradient of the Maxwell nanoliquid increase with increasing rotation number (λ) in both the suction and non-suction cases. The heat transfer rate decreases for $V0 \neq 0$ but increases for $V0 = 0$ as λ increases. The mass transfer rate, heat transfer rate and velocity gradient of the rotating Maxwell nanoliquid decrease with the increasing β for both $V0 = 0$ and $V0 \neq 0$. The dimensionless value of $-\theta'(0)$ decreases as R increases in both the suction and non-suction cases. However, $-\phi'(0)$ and $f''(0)$ increase with the increasing R in both cases. The dimensionless values of $-\phi'(0)$ and $f''(0)$ increase with the increasing Nb for both $V0 = 0$ and $V0 \neq 0$. The heat-transfer rate decreases with the increasing Nb.

The dimensionless velocity gradient increases for $V0 \neq 0$ but decreases for $V0 = 0$ as Nt increases. The Sherwood number and temperature gradient decrease in both cases with the increasing Nt. For $V0 \neq 0$, the velocity gradient increases, whereas it decreases for $V0 = 0$ as Cr increases. The value of $-\theta'(0)$ decreases, whereas $-\phi'(0)$ increases in both cases with the increasing Cr. The increasing $E1$ increases $f''(0)$ for $V0 \neq 0$ but decreases it for $V0 = 0$. The Nusselt number decreases in the suction case and increases in the non-suction case as $E1$ increases. The species concentration gradient decreases in both cases with the increasing $E1$. The velocity gradient increases for $V0 \neq 0$ but decreases for $V0 = 0$ as δ increases. The value of $-\theta'(0)$ decreases, whereas $-\phi'(0)$ increases in both cases with the increasing δ. The skin friction coefficient increases for $V0 \neq 0$ but decreases for $V0 = 0$ as B1 increases. Finally, $-\theta'(0)$ increases, whereas $-\phi'(0)$ decreases in both cases as B1 increases.

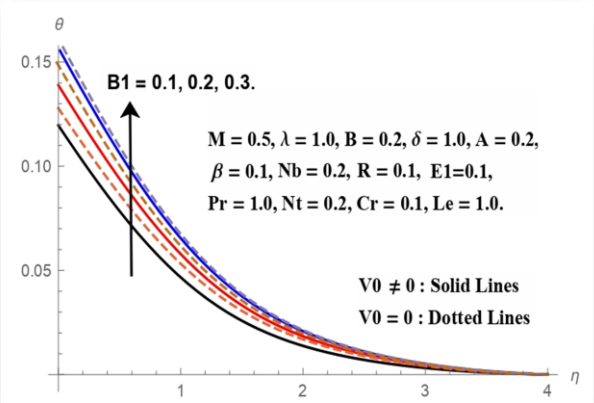


Fig. 24. Effect of B1 on θ.

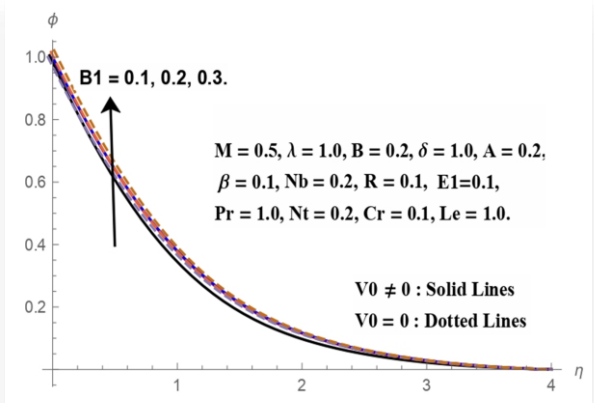


Fig. 25. Effect of B1 on ϕ.

5. Conclusions

A comparative analysis of the diffusion of species and energy transport features of rotating Maxwell nanoliquid flow over an elongating exponential surface with and without suction, by taking boundary condition of convective type into account, is presented in this article. The finite element method is utilised to solve the dimensionless equations of mass, heat and momentum. Velocity sketches in x and y directions, concentration and temperature sketches for dissimilar values of parameters are examined in detail and important summaries are mentioned below.

(i) An increase in the activation energy parameter leads to a significant magnification in the concentration profiles of the nanoliquid for both suction ($V0 \neq 0$) and non-suction ($V0 = 0$) cases.

Table 3. The effect of various parameters on skin-friction coefficient $f''(0)$, local Nusselt number $-\theta'(0)$ and local Sherwood number $-\phi'(0)$.

Parameter					$f''(0)$		$-\theta'(0)$		$-\phi'(0)$	
M	λ	β	R	Nb	$V0 \neq 0$	$V0 = 0$	$V0 \neq 0$	$V0 = 0$	$V0 \neq 0$	$V0 = 0$
0.1	1.0	0.2	0.1	0.2	−0.70118	−1.14140	0.08804	0.08615	0.87140	0.74857
0.4	1.0	0.2	0.1	0.2	−0.90632	−1.26921	0.08671	0.08574	0.78171	0.73018
0.7	1.0	0.2	0.1	0.2	−1.14140	−1.38860	0.08610	0.08540	0.74857	0.71433
0.5	1.0	0.2	0.1	0.2	−0.70118	−0.69482	0.08804	0.08721	0.86407	0.81146
0.5	1.4	0.2	0.1	0.2	−0.55695	−0.54695	0.08802	0.08802	0.87490	0.86490
0.5	1.7	0.2	0.1	0.2	−0.53901	−0.53901	0.08801	0.08826	0.88205	0.88205
0.5	1.0	0.1	0.1	0.2	−0.70118	−0.69482	0.08804	0.08721	0.87140	0.81146
0.5	1.0	0.2	0.1	0.2	−0.70809	−0.70809	0.08719	0.08719	0.80971	0.80970
0.5	1.0	0.3	0.1	0.2	−0.72105	−0.72105	0.08716	0.08716	0.80796	0.80796
0.5	1.0	0.2	0.1	0.2	−0.70118	−0.69482	0.08804	0.08721	0.81140	0.81146
0.5	1.0	0.2	0.3	0.2	−0.69482	−0.69325	0.08623	0.08623	0.81445	0.81445
0.5	1.0	0.2	0.5	0.2	−0.68542	−0.69215	0.08534	0.08534	0.81717	0.81717
0.5	1.0	0.2	0.1	0.1	−0.70119	−0.68452	0.08851	0.08771	0.82079	0.76432
0.5	1.0	0.2	0.1	0.3	−0.69482	−0.67548	0.08559	0.08559	0.84055	0.84055
0.5	1.0	0.2	0.1	0.5	−0.68452	−0.66584	0.08239	0.08239	0.85183	0.85183

Table 4. The effect of various parameters on skin-friction coefficient $f''(0)$, local Nusselt number $-\theta'(0)$ and local Sherwood number $-\phi'(0)$.

Parameter					$f''(0)$		$-\theta'(0)$		$-\phi'(0)$	
Nt	Cr	$E1$	δ	B1	$V0 \neq 0$	$V0 = 0$	$V0 \neq 0$	$V0 = 0$	$V0 \neq 0$	$V0 = 0$
0.1	0.1	0.1	1.0	0.5	−0.70118	−0.69482	0.08807	0.08725	0.89504	0.83330
0.4	0.1	0.1	1.0	0.5	−0.69482	−0.69587	0.08709	0.08706	0.74664	0.74668
0.7	0.1	0.1	1.0	0.5	−0.65842	−0.70154	0.08688	0.08682	0.64094	0.64494
0.2	0.1	0.1	1.0	0.5	−0.70118	−0.69482	0.08804	0.08721	0.87140	0.81146
0.2	0.2	0.1	1.0	0.5	−0.69482	−0.69524	0.08801	0.08716	0.92748	0.92768
0.2	0.3	0.1	1.0	0.5	−0.67542	−0.70123	0.08711	0.08711	1.03152	1.03159
0.2	0.1	0.1	1.0	0.5	−0.70118	−0.69498	0.08804	0.08721	0.87140	0.81146
0.2	0.1	0.5	1.0	0.5	−0.69471	−0.70809	0.08729	0.08724	0.75819	0.75819
0.2	0.1	0.9	1.0	0.5	−0.67533	−0.72105	0.08725	0.08725	0.74797	0.74799
0.2	0.1	0.1	0.1	0.5	−0.70118	−0.69482	0.08804	0.08721	0.81140	0.81146
0.2	0.1	0.1	0.5	0.5	−0.69482	−0.70215	0.08721	0.08712	0.82706	0.82706
0.2	0.1	0.1	0.9	0.5	−0.68542	−0.75242	0.08720	0.08602	0.84254	0.84254
0.2	0.1	0.1	1.0	0.1	−0.70118	−0.68452	0.08804	0.08721	0.87407	0.81146
0.2	0.1	0.1	1.0	0.2	−0.69482	−0.69521	0.09472	0.09472	0.80817	0.80817
0.2	0.1	0.1	1.0	0.3	−0.68321	−0.70215	0.10203	0.10203	0.80496	0.80496

(ii) The magnetic parameter induces a Lorentz force that retards fluid motion (decreasing velocity) while simultaneously elevating the liquid's temperature due to the additional work required to overcome the force.

(iii) Higher values of the rotation parameter led to a degradation in temperature distributions, a trend that is more pronounced in the presence of suction.

(iv) The temperature of the rotating Maxwell nanoliquid magnifies with the magnifying values of β both without and with suction.

(v) With the amplifying values of thermal Biot number (B1), the temperature profiles of the Maxwell nanoliquid increase.

References

[1] Choi, S.U.S., Zhang, Z.G., Yu, W., Lockwood, F.E., & Grulke, E.A. (2001). Anomalous thermal conductivity enhancement in nanotube suspensions. *Applied Physics*, 79(14), 2252–2254. doi: 10.1063/1.1408272

[2] Ghalambaz, M., Behseresht, A., Behseresht, J., & Chamkha, A.J. (2015). Effects of nanoparticles diameter and concentration on natural convection of the Al_2O_3-water nanofluids considering variable thermal conductivity around a vertical cone in porous media. *Advanced Powder Technology*, 26(1), 224–235. doi: 10.1016/j.apt.2014.10.001

[3] Ghalambaz, M., Doostani, A., Chamkha, A.J., & Ismael, M.A. (2017). Melting of nanoparticles-enhanced phase-change materials in an enclosure: effect of hybrid nanoparticles. *International journal of Mechanical Sciences*, 134, 85–97. doi: 10.1016/j.ijmecsci.2017.09.045

[4] Saha, S., Raut, S., & Das, A.N. (2021). Thermal enhancement and entropy generation of laminar water-Al_2O_3 nanofluid flow through a sudden expansion channel with bell-shaped surface. *International Journal of Fluid Mechanics Research*, 48(4), 65–78. doi: 10.1615/InterJFluidMechRes.2021039636

[5] Sudarsana Reddy, P., Sreedevi, P., & Chamkha, A.J. (2018). MHD boundary layer heat and mass transfer characteristics of

nanofluid over a vertical cone under convective boundary condition. *Propulsion and Power Research*, 7(4), 308–319. doi: 10.1016/j.jppr.2018.11.004

[6] Fadodun, O.G., Amosun, A.A., Salau, A.O., Olaloye, D.O., Ogundeji, J.A., Ibitoye, F.I., & Balogun, F.A. (2020). Numerical investigation and sensitivity analysis of turbulent heat transfer and pressure drop of Al_2O_3/H_2O nanofluid in straight pipe using response surface methodology. *Archives of Thermodynamics*. 41(1), 3–30. doi: 10.24425/ather.2020.132948

[7] Iweka, S.C., & Fadodun, O.G. (2021). Numerical modeling of heat transfer in Al_2O_3/H_2O nanofluid flowing through a Bessel-like converging pipe. *Archives of Thermodynamics*, 42(2), 121–153. doi: 10.24425/ather.2021.137557

[8] Rashad, A.M., & Mansour, M.A. (2022). Natural Bioconvective Flow Through a Vertical Cylinder in Porous Media Drenched with a Nanofluid. *Journal of Nanofluids*, 11(3), 340–349. doi: 10.1166/jon.2022.1854

[9] Chamkha, A.J., Nabwey, H.A., Abdelrahman, Z.M.A., & Rashad, A.M. (2020). Mixed Bioconvective Flow Over a Wedge in Porous Media Drenched with a Nanofluid. *Journal of Nanofluids*, 9(1), 24–35. doi: 10.1166/jon.2020.1728

[10] Sreedevi, P., Sudarsana Reddy, P., & Sheremet, M.A. (2020). Impact of homogeneous-heterogeneous reactions on heat and mass transfer flow of Au-Eg and Ag-Eg Maxwell nanofluid past a horizontal stretched cylinder. *Journal of Thermal Analysis and Calorimetry*, 141(1), 533–546. doi: 10.1007/s10973-020-09581-3

[11] Ahmed, J., Khan, M., & Ahmad, L. (2019). Stagnation point flow of Maxwell nanofluid over a permeable rotating disk with heat source/sink. *Journal of Molecular Liquids*, 287, 110853. doi: 10.1016/j.molliq.2019.04.130

[12] Ijaz, M., & Ayub, M. (2019). Nonlinear convective stratified flow of Maxwell nanofluid with activation energy. *Heliyon*, 5(1), e01121. doi: 10.1016/j.heliyon.2019.e01121

[13] Ahmed, J., Khan, M., Ahmad, L., Alzahrani, A.K., & Alghamdi, M. (2019). Thermally radiative flow of Maxwell nanofluid over a permeable rotating disk. *Physica Scripta*, 94(12), 125016. doi: 10.1088/1402-4896/ab3b9a

[14] Ahmed, A., Khan, M., Ahmed, J., Hafeez, A., & Iqbal, Z. (2020). Unsteady stagnation point flow of Maxwell nanofluid over stretching disk with Joule heating. *Arabian Journal for Science and Engineering*, 45(7), 5529–5540. doi: 10.1007/s13369-020-04468-9

[15] Ahmed, A., Khan, M., & Ahmed, J. (2020). Mixed convective flow of Maxwell nanofluid induced by vertically rotating cylinder. *Applied Nanoscience*, 10(12), 5179–5190. doi: 10.1007/s13204-020-01320-2

[16] Sharma, R., Hussain, S.M., Raju, C.S.K., Seth, G.S., & Chamkha, A.J. (2020). Study of graphene Maxwell nanofluid flow past a linearly stretched sheet: A numerical and statistical approach. *Chinese Journal of Physics*, 68, 671–683. doi: 10.1016/j.cjph.2020.10.013

[17] Khan, M.N., & Nadeem, S. (2020). Theoretical treatment of bioconvective Maxwell nanofluid over an exponentially stretching sheet. *Canadian Journal of Physics*, 98(8), 732–741. doi: 10.1139/cjp-2019-0380

[18] Abro, K.A., Soomro, M., Atangana, A., & Gómez-Aguilar, J.F. (2022). Thermophysical properties of Maxwell nanofluids via fractional derivatives with regular kernel. *Journal of Thermal Analysis and Calorimetry*, 147(1), 449–459. doi: 10.1007/s10973-020-10287-9

[19] Ali, R., Asjad, M.I., Aldalbahi, A., Rahimi-Gorji, M., & Rahaman, M. (2021). Convective flow of a Maxwell hybrid nanofluid due to pressure gradient in a channel. *Journal of Thermal Analysis and Calorimetry*, 143(2), 1319–1329. doi: 10.1007/s10973-020-10304-x

[20] Jamshed, W. (2021). Numerical investigation of MHD impact on Maxwell nanofluid. *International Communications in Heat and Mass Transfer*, 120, 104973. doi: 10.1016/j.icheatmasstransfer.2020.104973

[21] Gowda, R.J.P., Rauf, A., Naveen Kumar, R., Prasannakumara, B.C., & Shehzad, S.A. (2022). Slip flow of Casson–Maxwell nanofluid confined through stretchable disks. *Indian Journal of Physics*, 96(7), 2041–2049. doi: 10.1007/s12648-021-02153-7

[22] Zhou, S.S., Bilal, M., Khan, M.A., & Muhammad, T. (2021). Numerical analysis of thermal radiative Maxwell nanofluid flow over-stretching porous rotating disk. *Micromachines*, 12(5), 540. doi: 10.3390/mi12050540

[23] Mustafa, M. (2015). Cattaneo-Christov heat flux model for rotating flow and heat transfer of upper-convected Maxwell fluid. *AIP Advances*, 5(4), 047109. doi: 10.1063/1.4917306

[24] Ahuja, J., & Gupta, U. (2016). MHD effects for a rotating nanofluid layer for LTNE model. *International Journal of Technology*, 6(2), 209. doi: 10.5958/2231-3915.2016.00032.8

[25] Hayat, T., Muhammad, T., Shehzad, S.A., & Alsaedi, A. (2017). Three dimensional rotating flow of Maxwell nanofluid. *Journal of Molecular Liquids*, 229, 495–500. doi: 10.1016/j.molliq.2016.12.095

[26] Rashid, S., Khan, M.I., Hayat, T., Ayub, M., & Alsaedi, A. (2020). Darcy–Forchheimer flow of Maxwell fluid with activation energy and thermal radiation over an exponential surface. *Applied Nanoscience*, 10(8), 2965–2975. doi: 10.1007/s13204-019-01008-2

[27] Ali, B., Nie, Y., Hussain, S., Manan, A., & Sadiq, M.T. (2020). Unsteady magneto-hydrodynamic transport of rotating Maxwell nanofluid flow on a stretching sheet with Cattaneo–Christov double diffusion and activation energy. *Thermal Science and Engineering Progress*, 20, 100720. doi: 10.1016/j.tsep.2020.100720

[28] Ahmed, A., Khan, M., Ahmed, J., & Hafeez, A. (2020). Von Kármán rotating flow of Maxwell nanofluids featuring the Cattaneo-Christov theory with a Buongiorno model. *Applied Mathematics and Mechanics*, 41(8), 1195–1208. doi: 10.1007/s10483-020-2632-8

[29] Khalid, I.K., Mokhtar, N.F.M., Ibrahim, Z.B., & Siri, Z. (2020). Rayleigh–Bénard convection in Maxwell nanofluids layer saturated in a rotating porous medium with feedback control subjected to viscosity and thermal conductivity variations. *Applied Nanoscience*, 10(8), 3085–3095. doi: 10.1007/s13204-020-01302-4

[30] Ramaiah, K.D., Surekha, P., Kotha, G., & Thangavelu, K. (2020). MHD rotating flow of a Maxwell fluid with Arrhenius activation energy and non-Fourier heat flux model. *Heat Transfer*, 49(4), 2209–2227. doi: 10.1002/htj.21717

[31] Khan, M.N., & Nadeem, S. (2021). A comparative study between linear and exponential stretching sheet with double stratification of a rotating Maxwell nanofluid flow. *Surfaces and Interfaces*, 22, 100886. doi: 10.1016/j.surfin.2020.100886

[32] Ali, B., Pattnaik, P.K., Naqvi, R.A., Waqas, H., & Hussain, S. (2021). Brownian motion and thermophoresis effects on bioconvection of rotating Maxwell nanofluid over a Riga plate with Arrhenius activation energy and Cattaneo-Christov heat flux theory. *Thermal Science and Engineering Progress*, 23, 100863. doi: 10.1016/j.tsep.2021.100863

[33] Chu, Y.M., Ramzan, M., Shaheen, N., Dong Chung, J., Kadry, S., Howari, F., Malik, M.Y., & Ghazwani, H.A.S. (2021). Analysis of Newtonian heating and higher-order chemical reaction on a Maxwell nanofluid in a rotating frame with gyrotactic microor-

ganisms and variable heat source/sink. *Journal of King Saud University-Science*, 33(8), 101645. doi: 10.1016/j.jksus.2021.101645

[34] Alzahrani, F., & Ijaz Khan, M. (2021). Applications of Darcy-Forchheimer 3D reactive rotating flow of rate type nanoparticles with non-uniform heat source and sink and activation energy. *Chemical Physics Letters*, 783, 139054. doi: 10.1016/j.cplett.2021.139054

[35] Cao, L., Zhang, P., & Si, X. (2022). Electroosmotic flow of two-layer fluid containing Oldroyd-B fluid with fractional derivative in a rotating microparallel channel. *Microfluidics and Nanofluidics*, 26(5), 34. doi: 10.1007/s10404-022-02539-x

[36] Wei, Y., Rehman, S.U., Fatima, N., Ali, B., Ali, L., Chung, J.D., & Shah, N.A. (2022). Significance of dust particles, nanoparticles radius, coriolis and lorentz forces: The case of Maxwell dusty fluid. *Nanomaterials*, 12(9), 1512. doi: 10.3390/nano12091512

[37] Ali, B., Thumma, T., Habib, D., Salamat, N., & Riaz, S. (2022). Finite element analysis on transient MHD 3D rotating flow of Maxwell and tangent hyperbolic nanofluid past a bidirectional stretching sheet with Cattaneo-Christov heat flux model. *Thermal Science and Engineering Progress*, 28, 101089. doi: 10.1016/j.tsep.2021.101089

[38] Raza, J., Mustafa, F., Lund, L.A., Shah, Z., Alshehri, M.H., & Vrinceanu, N. (2024). Optimization of heat transfer rate of trihybrid nanofluid embedded between two horizontal coaxial cylinders by RSM. *Case Studies in Thermal Engineering*, 60, 104637. doi: 10.1016/j.csite.2024.104637

[39] Shutaywi, M., Raza, J., Lund, L.A., Shah, Z., Vrinceanu, N., & Deebani, W. (2024). Optimization of heat transfer in a channel with stretching walls using a magnetized tetra-hybrid nanofluid. *Advances in Mechanical Engineering*, 16(11). doi: 10.1177/16878132241293959

[40] Shutaywi, M., Raza, J., Abualnaja, K.M., Shah, Z., Vrinceanu, N., & Deebani, W. (2025). Integrated Taguchi-GRA-PCA for optimizing the heat transfer performance of trihybrid Casson nanofluid flow over stretching sheet with quadratic velocity. *Journal of Radiation Research and Applied Sciences*, 18(3), 101570. doi: 10.1016/j.jrras.2025.101570

[41] Raza, J., & Ashfaq, A. (2025). Optimization of heat transfer in two-phased nanofluid flow over a biaxial sheet using Taguchi-GRA method. *Multiscale and Multidisciplinary Modeling Experiments and Design*, 8(1), 124. doi: 10.1007/s41939-024-00712-z

[42] Sudarsana Reddy, P., & Chamkha, A.J. (2016). Soret and Dufour Effects on unsteady MHD heat and mass transfer over a stretching sheet with thermophoresis and non-uniform heat generation/absorption. *Journal of Applied Fluid Mechanics*, 9(5), 2443–2455. doi: 10.18869/acadpub.jafm.68.236.25171

[43] Sreedevi, P., Sudarsana Reddy, P., & Chamkha, A.J. (2017). Heat and Mass transfer analysis of nanofluid over linear and non- linear stretching surface with thermal radiation and chemical reaction. *Powder Technology*, 315, 194–204. doi: 10.1016/j.powtec.2017.03.059

[44] Sudarsana Reddy, P., Chamkha, A.J., & Al-Mudhaf, A. (2017). MHD heat and mass transfer flow of a nanofluid over an inclined vertical porous plate with radiation and heat generation/absorption. *Advanced Powder Technology*, 28(3), 1008–1017. doi: 10.1016/j.apt.2017.01.005

[45] Sudarsan Reddy, P., & Prasada Rao, V. (2012). Thermo-diffusion and diffusion –thermo effects on convective heat and mass transfer through a porous medium in a circular cylindrical annulus with quadratic density temperature variation – Finite element study. *Journal of Applied Fluid Mechanics*, 5(4), 139–144. doi: 10.36884/jafm.5.04.19472

[46] Sudrsana Reddy, P., Sreedevi, P., & Chamkha, A.J. (2017). MHD boundary layer flow, heat and mass transfer analysis over a rotating disk through porous medium saturated by Cu-water and Ag-water nanofluid with chemical reaction. *Powder Technology*, 307, 46–55. doi: 10.1016/j.powtec.2016.11.017